

GaussianHair: Hair Modeling and Rendering with Light-aware Gaussians

Haimin Luo^{1,4} Min Ouyang^{1,3} Zijun Zhao^{1,3} Suyi Jiang¹ Longwen Zhang^{1,3}
 Qixuan Zhang^{1,3} Wei Yang² Lan Xu^{1*} Jingyi Yu^{1*}
¹ShanghaiTech University ²Huazhong University of Science and Technology
³Deemos Technology ⁴LumiAni Technology



Figure 1. **Illustration of Our GaussianHair.** We introduce “GaussianHair”, a novel hair representation technique that conceptualizes a hair strand as a series of connected cylindrical 3D Gaussians. This representation facilitates the effective reconstruction of hair strands from videos captured using handheld smartphones, while also supporting an efficient scattering model. Leveraging the “GaussianHair” framework, image-based hair modeling extends beyond mere reconstruction, enabling advanced functionalities such as hair editing, relighting, and dynamic rendering.

Abstract

Hairstyle reflects culture and ethnicity at first glance. In the digital era, various realistic human hairstyles are also critical to high-fidelity digital human assets for beauty and inclusivity. Yet, realistic hair modeling and real-time rendering for animation is a formidable challenge due to its sheer number of strands, complicated structures of geometry, and sophisticated interaction with light. This paper presents GaussianHair, a novel explicit hair representation. It enables comprehensive modeling of hair geometry and appearance from images, fostering innovative illumination effects and dynamic animation capabilities. At the heart of GaussianHair is the novel concept of representing each hair strand as a sequence of connected cylindrical 3D Gaussian primitives. This approach not only retains the hair’s ge-

ometric structure and appearance but also allows for efficient rasterization onto a 2D image plane, facilitating differentiable volumetric rendering. We further enhance this model with the “GaussianHair Scattering Model”, adept at recreating the slender structure of hair strands and accurately capturing their local diffuse color in uniform lighting. Through extensive experiments, we substantiate that GaussianHair achieves breakthroughs in both geometric and appearance fidelity, transcending the limitations encountered in state-of-the-art methods for hair reconstruction. Beyond representation, GaussianHair extends to support editing, relighting, and dynamic rendering of hair, offering seamless integration with conventional CG pipeline workflows. Complementing these advancements, we have compiled an extensive dataset of real human hair, each with meticulously detailed strand geometry, to propel further research in this

field.

1. Introduction

Hairstyles serve as visible and tangible representations of diversity in culture and ethnicity. For example, the intricate braiding patterns in traditional African hairstyles not only serve as a symbol of ethnic identity but also often carry cultural significance whereas the Sari Braid of India is commonly associated with traditional attire and serves as a symbol of cultural elegance. In the digital era, embracing a variety of hairstyles in the cyber world further helps to challenge narrow beauty standards, promote inclusivity, and contribute to a more accurate and respectful representation of human culture. Generating realistic digital versions of these hairstyles, however, remains challenging. Traditional modeling tools require extensive experience and labor to replicate the intricate details of different hair types, such as curly, straight, wavy, or coiled. Plausible hairstyle models should further conveniently support high-quality rendering to faithfully reflect their original color, texture, light penetration scattering, etc, at a high level of detail and under dynamic movements.

Over the past two decades, our community has witnessed the evolution of hair modeling from explicit reconstruction methods to implicit neural representation, leveraging advances in neural modeling and rendering. Explicit geometry such as 3D polylines, or strands, has served as the dominant representation for faithful hair rendering and simulation [2, 6, 18, 61, 85]. These methods involved explicitly defining the geometry and properties of each individual hair strand. Building such models either relies on experienced artists or requires using expensive apparatus (e.g., with dense synchronized cameras, controlled lighting, etc) to achieve strand-accurate hair geometry and reflectance properties [21, 33, 50, 68]. They have by far been restricted to laboratory settings and cannot be readily deployed to acquire many real hairstyles in daily life. The rise of deep learning and neural networks has led to a shift towards implicit neural representation for modeling complex structures like hair. Such methods [4, 48, 49] unanimously aim to learn a function that directly maps input coordinates to output values without explicitly representing the underlying geometry. They are more flexible and adaptive, computationally efficient, and achieve a certain level of realism. However, implicit representations have their limitations, ranging from limited inability to produce photorealistic relighting, to difficulties in animating the hair, and to compatibility issues with traditional computer graphics (CG) pipeline workflows.

In recent advancements, hybrid representation methodologies have emerged at the forefront in the realm of image-based hair modeling. These methods ingeniously bind

appearance features to three-dimensional proxies such as strands and points [62, 70], or to more coarse geometrical forms [67]. This process involves differentially rendering these proxies into two-dimensional features, which are then intricately decoded into hair appearance through neural rendering techniques. Notably, Neural Strands [62] epitomizes this approach with a strand-based generative model, learned from synthetic data. It adeptly decodes feature vectors, encoded as UV textures on the scalp, into meticulously detailed hair strands corresponding to specific scalp locations. Following in these innovative footsteps, Neural Haircut [67] takes this strategy further by reconstructing the implicit surfaces of the head and shoulders. It then performs strand-level hair reconstruction with priors learned from synthetic datasets. However, the rendering process of these methods involves the transformation of strand representation back into feature maps, necessitating a substantial reliance on neural renderers for final appearance rendering. Such reliance inherently restricts their ability to perform per-strand animation, a key aspect in achieving dynamic and lifelike representations of hair.

In line with current research trends, we posit that an effective representation for hair modeling hinges on two key aspects: a geometry proxy model that conforms to the thin and elongated structure of hair fibers, as well as an efficient scattering and deformation model for photo-realistic hair relighting and animation. The seminal work, 3D Gaussian Splatting (3DGS) by Kerbl et al. [27] uses a set of volumetric Gaussians with spherical harmonics appearance parameters to model 3D scenes, which brings new possibility for hair modeling. Akin to 3DGS, in this paper, we introduce *GaussianHair*, a novel hair modeling and rendering scheme via light-aware Gaussian splatting. As shown in Fig. 1, from only video inputs using handheld devices, our *GaussianHair* achieves strand-level hair reconstruction and scattering effects for vivid hair rendering, editing, relighting, and dynamic animation.

In *GaussianHair*, we adopt a novel primitive, dubbed cylindrical 3D Gaussian. This primitive, a 3D Gaussian with a considerably smaller radius relative to its length, allows each hair strand to be depicted as a sequence of linked cylindrical 3D Gaussian primitives, optimized through photometric supervision. This chain of connected cylindrical Gaussians adeptly retains both the geometric structure and appearance attributes of hair, such as color and opacity, facilitating efficient rasterization onto a 2D image plane for differentiable volumetric rendering. To effectively model hair strands from images, we initialize a set of cylindrical 3D Gaussians with a fixed small radius, sampled from points on head and hair meshes, optimizing them via differentiable rasterization. With additional guidance on 2D orientations, we derive an Oriented 3D Gaussian Field (O3GF), subsequently used to optimize geometry tex-



Figure 2. **Illustration of our RealHair dataset.** Our RealHair dataset represents a comprehensive and culturally diverse collection of human hairstyles, encompassing a variety of distinctive styles reflective of global hair characteristics. It comprises 281 high-resolution (4K) videos, totaling approximately 3000 frames, each meticulously annotated with detailed geometry segmentations and individual hair strand information.

ture for generating coarse hair strands from a pre-trained hair strand decoder, following the approach of Neural Hair-cut [67]. A cylindrical 3D Gaussian is then assigned to each section between two adjacent nodes of a coarse hair strand, creating a connected sequence. We then perform further refinement to optimize the GaussianHair model.

The visual appearance of hair is significantly influenced by accurately modeling how light reflects and scatters through the hair volume. Our reconstructed GaussianHair, conforming to the thin and elongated structure of hair strands, facilitates the establishment of a scattering model. We employ the sophisticated UE4 approximated scattering function of the Marschner Hair Model [45] to simulate light scattering for the incident and exitant directions and provide an extra transmittance term to assess the light reaching each Gaussian. Our GaussianHair representation extends to support editing, relighting, and dynamic rendering of hair, offering seamless integration with conventional CG pipeline workflows, a breakthrough unseen in prior methods. Benefiting from the efficient capture setup and the strong representational ability of GaussianHair, we have compiled an extensive dataset of real human hair, each meticulously cap-

turing detailed strand geometry, to foster further research in this field, as shown in Fig. 2. We conduct extensive qualitative and quantitative experiments of GaussianHair on our diverse dataset, to demonstrate the effectiveness of GaussianHair for vivid hair modeling and rendering.

2. Related Work

Hair modeling remains challenging for computer graphics due to the geometric complexity of natural hair, its sophisticated interaction with light for realistic rendering, and the high computational demands for hair animations. Attempts to address these key issues come from both the modeling and rendering communities and the imaging and photography ones.

Geometric Modeling . Early works aim to employ some type of parametric representation of hair that provides an interface to modeling hair shape. Examples include representing hair groups as 2D parametric surfaces [30, 36, 51], wisps and generalized cylinders [12, 13, 58, 79, 81], multi-resolution cylinders [28, 72] or hair meshes [86]. Although hair shape-curving tools have become convenient, creat-

ing natural hairstyles such as the ones shown in this paper still requires tedious labor. A number of approaches have hence sought to reconstruct hair strands using computer vision techniques such as multi-view stereo (MVS). Such approaches, often referred to as image-based, include early direct reconstruction attempts [31] as well as 3D volume-based solutions [15, 54] that generate strands in a heuristic manner. Subsequent approaches [43, 44, 55, 77] have focused on using tailored acquisition apparatus, e.g., tailored imaging systems, for better reconstructing the 3D orientation field. They then triangulate the results in 3D space and grow corresponding strands. Shape primitives, e.g., ribbons, wisps, and strands, are further utilized to fit the point cloud as structure guidance[3]. LPMVS [50] further introduces a line-based PatchMatch MVS algorithm to more reliably reconstruct the point cloud alongside the actual hair strand. The point clouds are then connected into hair strands. Based on LPMVS, Sun et al. [68] adopts a per-pixel light code to further estimate the albedo color and reflectance of the captured hair for realistic rendering. All these approaches have focused mainly on the visible part of hair strands, i.e., hair strands at the outer regions while leaving out the interior hair volume as their reconstructions are generally noisy due to occlusions. Several data-driven methods [19, 20, 84, 89] hence attempt to first build a hairstyle database that includes both the inner and outer geometry and then search for hair models from the database that best match the visible hair region. The recent deep learning-based approaches [32, 62, 63, 67, 78, 80, 94] learn hair shape prior on synthetic hair dataset and can efficiently infer the entire hair volume, e.g., 3D orientation, even from a few images. However, these data-driven approaches rely heavily on the varieties and the quality of hairstyles of the training data. By far, public hairstyle datasets are still scarce and the only available ones [25, 26, 66, 93] contain few varieties and relatively simple styles, far from the richness and diversity we observe in real life. We demonstrate that our GaussianHair representation provides a viable path to produce very high-quality hairstyles using a hand-held device. Further, we provide a new, large hairstyle dataset Fig. 2 that contains not only geometry but also appearance.

Neural Implicit Representation. It is worth mentioning that besides explicit geometry, hairstyles can also be modeled using implicit representations.

Such representations aim to learn continuous implicit functions from the acquired multi-view images that map spatial locations or features to some properties with Multi-Layer Perceptrons (MLPs), e.g., signed distance [9, 23, 56, 71, 73, 92], occupancy field [17, 22, 47, 59, 64] or radiance field [5, 37, 46, 48]. Theoretically, they can handle extremely complex geometry and complicated appearance details such as hair as they eliminate the need for mod-

eling the topology of hairstyles. For example, Wu et al. [78] exploits a voxel-aligned implicit function to predict 3D hair features, e.g., orientations and occupancies and further adopts an implicit hair growing scheme to obtain the complete strand model. Its concurrent work Kuang et al. [32] adopts a multi-view transformer to predict the orientation and occupancy fields. ConvNeRF [41] further combines the Neural Radiance Field (NeRF) [48] and a UNet renderer for high-quality static hair geometry modeling and rendering. However, these approaches cannot readily handle re-rendering tasks such as re-lighting or hair animation.

Potentially, subsequent variants of NeRF [4, 10, 41, 49, 69] can be deployed to conduct re-lighting [5, 7, 82, 87, 91] or even handle dynamic scenes [8, 57, 60]. For example, Artemis [42] achieves high-quality rendering of animated animal fur driven by body movements. However, it can only handle short hair that generally does not bend or fold. Applying re-lightable NeRF to hairstyles is largely missing as most relighting tasks aim to modify low-frequency components whereas hair relighting requires as detail as specularity and scattering through individual fibers that are difficult to model using implicit representations.

Volume/Point Representations. As a NeRF can be converted back to a volume representation, several acceleration schemes have been proposed to conduct real-time rendering, ranging from Plenotree [83] to the more recent Mixture of volumetric primitives (MVP) [40]. By representing scenes as a compact set of voxels., MVP mitigates the rendering artifacts caused by the limited volume resolution. Followup works [74, 75] extend the MVP to capturing dynamic human hair by binding voxels alongside the hair strands, achieving both hair editing and dynamic simulation. However, their rendering quality is still bound by the size of the voxels and cannot readily match photographic quality rendering. The seminal work of Kerbl et al. [27] 3D Gaussian Splatting (3DGS) introduced Gaussian volumes as a new alternative to either mesh-based or neural-based scene representations. Its core idea of using a set of volumetric Gaussians, each with spherical harmonics appearance parameters, to model a 3D scene is revolutionary. 3DGS is also transformative as it not only achieves comparable rendering quality to NeRF and Instant-NGP [49] at an interactive speed but more importantly it eliminates the need to use MLP neural networks and hence can be implemented on low-end graphics hardware. 3DGS has since inspired numerous subsequent extensions [11] to model human avatars, dynamic scenes, and environment-responsive models. We aim to develop a 3DGS for hair. However, the challenges are multifold. First, as hair contains tens to hundreds of thousands of fibers, the direct Gaussian representations would be prohibitively dense and large on real hairstyles. Second, even if we manage to employ 3DGS

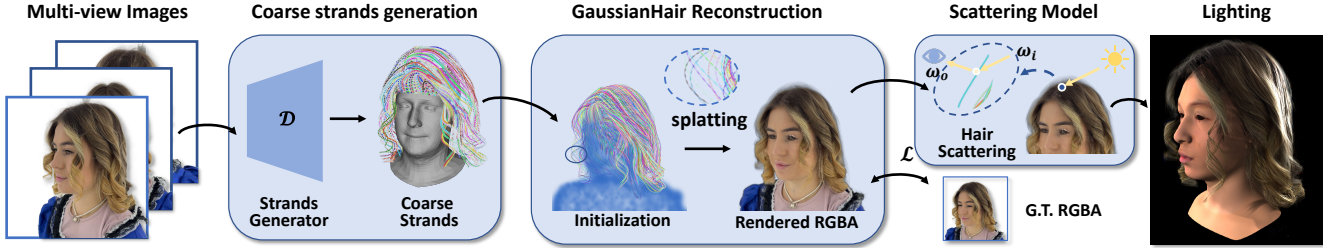


Figure 3. **Overview.** Our method employs a multi-stage process for hair modeling. Initially, an off-the-shelf decoder extracts coarse hair strands from multi-view images, which are then refined using differentiable strand-based splatting. This optimization aligns the rendered images with the ground truth. Finally, we apply a scattering model to the optimized strands, enhancing their relighting and dynamics modeling capabilities.

reconstruction on hair, the resulting representations are not easily animatable nor re-lightable.

We observe that 3DGS can be viewed as a special type of geometry proxy deployed in earlier image-based modeling and rendering techniques. Methods such as Light Field [34] and Lumigraph [14] use proxies such as planes, boxes, polygonal meshes, etc, to better conduct ray interpolation. For hair strands, we set out to employ a new type of primitive, a sequence of linked cylindrical 3D Gaussian, as proxies. A major advantage of this representation is that one can easily animate hair strands and potentially conduct physical-based rendering. Our work is also inspired by the latest approaches that incorporate points [62, 70] or meshes [67] as geometry primitives and convolutional renderers for appearance modeling. Such methods enable geometry editing but cannot modify appearance since the renderer only “memorizes” the baked hair appearance. Most related to ours, Wang et al. [76] directly exploits adaptive shells to bind the volumetric region for real-time rendering and companioned animation and simulation based on mesh. The key difference is they still adopt the implicit function to represent the short hair/fur, and thus can not conduct per-strand animation and simulation.

3. GaussianHair Representation

Traditional human hair modeling for realistic animation, requiring detailed artist input to define each strand’s geometry and properties, is labor-intensive. Image-based hair modeling, an automated alternative, reconstructs hair from images or videos. However, this method typically relies on complex and costly setups like dense camera arrays with controlled lighting [43, 44, 55, 77], and struggles with photorealistic rendering due to its use of explicit geometric representations like 3D polylines or parametric 3D curves. Recent advances in neural implicit representations, such as NeRF, MipNeRF, and InstantNGP [4, 48, 49], demonstrate remarkable proficiency in photorealistic hair modeling but lack the explicit geometry necessary for animation. Hybrid methodologies [62, 67, 74, 75] blend explicit geometry with vox-

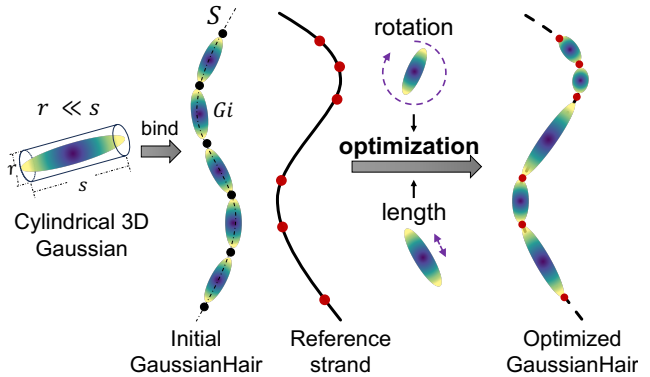


Figure 4. **Gaussian Hair Representation.** A hair strand is represented as a sequence of linked cylindrical 3D Gaussian primitives with their length s significantly larger than their diameter r . During the modeling process, initialized strands are optimized to the optimal structures.

els for animation, yet their coarse primitives hinder accurate hair lighting effects. Furthermore, these methods often require specialized neural renderers, developed for specific hair models during training [62, 67]. Although recent 3D Gaussian Splatting (3DGS) advancements [27] enable detailed scene reconstruction, their primitive structures are not naturally suited for hair strand modeling.

In response, we propose GaussianHair, an explicit volumetric hair representation optimized for both geometry and appearance. This approach leverages splatting rendering strategies to facilitate accurate hair modeling from images, allowing for dynamic animation and novel illumination. GaussianHair represents each hair strand as a sequence of linked cylindrical 3D Gaussian primitives, optimized in position, orientation, and length through photometric supervision, as illustrated in Fig. 4. We parameterize these primitives using directional vectors and scale factors. This series preserves hair’s geometric and appearance attributes and supports efficient rasterization for volumetric rendering. Critically, GaussianHair extracts explicit hair geom-

etry from images, addressing a significant gap in current research. To aid future work, we’ve compiled a dataset of authentic human hair, including 281 videos with about 3000 frames, each featuring detailed strand geometry.

Cylindrical Gaussian Hair Representation We define a hair strand \mathcal{S} explicitly as a sequence of cylindrical 3D Gaussian primitives, represented as $\mathcal{S} = \{G_i\}_{i=1}^L$, where each G_i corresponds to a segment of the hair strand. The individual cylindrical Gaussian G_i is characterized by its center position μ and covariance matrix Σ . The Gaussian function for a segment is given by:

$$G_i(x) = e^{-\frac{1}{2}(x-\mu)^T \Sigma^{-1}(x-\mu)}, \quad (1)$$

where x denotes a position in space. This formulation effectively segments the hair strand into L distinct parts, with each part modeled as a cylindrical Gaussian, capturing the intricate geometrical features of the hair strand.

The covariance matrix Σ_i for each cylindrical Gaussian is derived from the scaling matrix S and rotation matrix R , formulated as $\Sigma_i = R S S^T R^T$. Here, S is a diagonal matrix with diagonal elements $[d, d, s]$, representing the cylinder’s diameter and length, respectively. To maintain the characteristic cylindrical shape, the length s is set significantly larger than the diameter r . In our implementation, we use r with a value of $1.0e^{-4}$ to ensure this disparity. As a result, traditional hair strand parameters can be effectively integrated with our GaussianHair model. We represent each hair strand’s particles using one endpoint of the Gaussian, defined as $\mathbf{p}_i = \mu_i + \frac{1}{2}s_i \mathbf{d}_i$, where s_i is the length, and \mathbf{d}_i is the direction of the i th cylindrical Gaussian along the strand. The direction \mathbf{d}_i can be extracted from the last column of the rotation matrix R_i . This approach allows for the accumulation of hair strand node points from the cylindrical Gaussians, starting from the root position \mathbf{p}_0 on the scalp. To enhance the hair appearance model, each cylindrical Gaussian is also equipped with an opacity value α and a set of spherical harmonics (SH) coefficients. These coefficients represent view-dependent color c , adding further realism to the hair’s appearance and rendering.

During the rendering phase, all the cylindrical 3D Gaussians are projected onto the image space using the splatting technique. The color of each pixel is derived by accumulating the contributions from each Gaussian. This process involves transforming the 3D Gaussians into their 2D counterparts, denoted as g . The 2D covariance matrix for this transformation is defined as:

$$\Sigma' = J W \Sigma W^T J^T, \quad (2)$$

In this equation, J represents the Jacobian of the affine approximation of the projective transformation, and W denotes the view transformation matrix. The 2D mean, μ' ,

is calculated as the projected center of the Gaussian onto the image plane. The contribution of a Gaussian to a pixel u is then given as $w = g(u|\mu', \Sigma')\alpha$. Consequently, the rendered color \mathcal{C} of pixel u is accumulated as follows:

$$\mathcal{C} = \sum_{i \in N} T_i w_i c_i, \quad T_i = \prod_{j=1}^{i-1} (1 - w_j), \quad (3)$$

where N is the set of Gaussians contributing to the pixel. To facilitate efficient optimization of all trainable parameters, we employ a fast tile-based differentiable rasterizer [27]. In our implementation, the hair roots are fixed, and we optimize the other parameters, namely c , α , R , and S .

4. Image-based GaussianHair Modeling

With our GaussianHair representation, we facilitate the acquisition of detailed hair geometry and appearance directly from images captured quickly using a standard phone camera, as shown in Fig. 3. This approach circumvents the necessity for expensive and complex equipment typically used in traditional methods, such as camera arrays with controlled lighting setups.

Expedite Data Capture and Preprocessing. To demonstrate the ease and efficiency of our capture process, we detail a typical session. Utilizing the camera of a high-end mobile phone, specifically an iPhone 15 Pro Max, we capture a video of the subject’s hair at 4Kx60 FPS. During the capture, subjects are instructed to remain as still as possible. We conducted the video capture in two rounds as follows: in the first round, the camera was positioned approximately 1 meter away from the subject’s head, angled downward at about 30 degrees to focus on the hair’s upper portion, and another with the camera oriented horizontally. In both scenarios, the camera is swept in one direction, ensuring comprehensive coverage of the subject’s visible hair and upper torso for accurate data acquisition. Uniform white lighting is employed during the capture to facilitate precise texture recovery. From the captured videos, we uniformly select 80-100 frames and calibrate the camera’s intrinsic and extrinsic parameters using an off-the-shelf Structure from Motion (SfM) tool [1, 65]. For each frame, a set of Gabor filters is applied to compute a 2D orientation map \mathcal{O} [53]. Additionally, we generate a portrait alpha matte \mathcal{A} and a corresponding hair mask \mathcal{M} using pre-trained matting models [29, 38]. Furthermore, we fit a FLAME head model [35] and optimize a two-layer Instant-NSR [92] model, akin to Neural Haircut [67]. This process yields separable hair and body meshes, denoted as \mathbf{H} and \mathbf{B} respectively, which serve as geometry priors for the subsequent reconstruction phase.

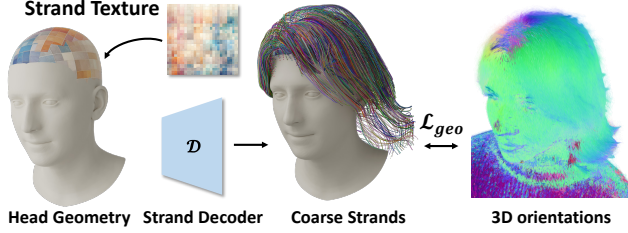


Figure 5. **Illustration of coarse strands generation.** Given fitted FLAME head mesh, we render a hair geometry texture in a differentiable manner with the 2D feature map as a UV map. Subsequently, an off-the-shelf decoder is utilized to obtain a set of hair strands which are then optimized to align with the actual hair geometry.

4.1. Oriented 3D Gaussian Field

The crux of our hair modeling technique lies in the precise recovery of individual hair strands from image data. Prior studies have focused on extracting directional points [62] or implicit orientation fields [67] solely from 2D orientation maps. In contrast, our approach involves generating accurate and comprehensive 3D Gaussian Orientation Fields to guide the initial creation of coarse hair strands, which are then refined in subsequent steps. We achieve this by reconstructing directional segments using additional RGB supervision with cylinder 3D Gaussians. More specifically, we generate a set of tiny 3D Cylinder Gaussians by sampling points from the reconstructed head and hair meshes, i.e., \mathbf{H} and \mathbf{B} respectively. We initialize the diameter of these Gaussians, r , to $1.0e^{-4}$ and set the length s to approximately 10 times the radius. During the optimization phase, we maintain a fixed value for r across all Gaussians, while optimizing the remaining parameters through differentiable rendering, in line with the standard 3DGS procedure. To accurately align cylinder Gaussian orientations with the natural hair strands, we render the orientations of Gaussians nearest to camera rays onto images and apply an orientation loss to minimize discrepancies, ensuring realistic hair representation.

$$\mathcal{L}_{\text{ori}} = \sum_{i,j} (1 - \mathcal{P}_i(\{\mathbf{d}\}, j) \cdot \mathcal{O}_i(j)), \quad (4)$$

where i represents the image index and j denotes a pixel within image i , $\mathcal{P}_i(\{\mathbf{d}\}, j)$ refers to the projection of the set of Gaussian directions $\{\mathbf{d}\}$ onto pixel j in image i . $\mathcal{O}_i(j)$ is the 2D orientation at pixel j in the orientation map \mathcal{O}_i . The symbol \cdot is used to denote the dot product operation. The total loss for optimizing our Oriented 3D Gaussian Field is defined as:

$$\mathcal{L}_{\text{ogf}} = \mathcal{L}_1 + \mathcal{L}_{\text{D-SSIM}} + \mathcal{L}_{\text{ori}}, \quad (5)$$

where \mathcal{L}_1 and $\mathcal{L}_{\text{D-SSIM}}$ are the photometric loss borrowed from the vanilla 3DGS, and all weighting factors are omit-

ted for clarity.

Although the generated OGF is composed of oriented cylinder Gaussians, these primitives are discrete in space and do not inherently form continuous hair strands. To address this, we focus on optimizing coarse hair strands derived from the OGF, as shown in Fig. 5. We employ a geometry texture, essentially a 2D feature map, to represent these coarse hair strands. This texture encodes information that can be decoded into lists of points along the hair strands, with their roots positioned on the scalp. The decoding process is facilitated by a Multi-Layer Perceptron (MLP) structured decoder, \mathcal{D} , following the methodology outlined in Neural Strands [62] and NeuralHirecuts [67]. Our primary goal is to generate coarse hair strands from the Oriented Gaussian Field (OGF), represented as \mathcal{O}^{3d} . To facilitate this, we first refine the OGF by excluding Gaussians situated inside the head geometry \mathbf{H} . This step is crucial to ensure that the subsequent hair strand modeling only involves Gaussian points relevant to hair geometry. Once the OGF is refined, we uniformly sample root points from the scalp area on the fitted FLAME head mesh \mathbf{H} . These root points are then used to construct the hair geometry texture \mathbf{z} . We decode this texture into a set of hair strand points \mathcal{P} , using the decoder \mathcal{D} . This approach, drawing upon techniques used in Neural Strands [62], effectively transforms the cleaned OGF into coarse hair strands, which are crucial for the accurate and realistic representation of hair.

$$\begin{aligned} \mathcal{L}_{\text{geo}} = & \sum_{\mathbf{p} \in \mathcal{P}} (\|\mathbf{p} - \mathbf{u}_o\|_2 + (1 - \mathbf{d}_p \mathbf{d}_o)) \Big|_{o=NN(\mathbf{p})} \\ & + \sum_{\mathbf{o} \in \mathcal{O}^{3d}} (\|\mathbf{u}_o - \mathbf{p}\|_2 + (1 - \mathbf{d}_o \mathbf{d}_p)) \Big|_{p=NN(\mathbf{o})}, \end{aligned} \quad (6)$$

where \mathbf{p} and \mathbf{o} are a point in \mathcal{P} and a Gaussian of \mathcal{O}^{3d} respectively, $\mathbf{o} = NN(\mathbf{p})$ means \mathbf{o} is the closest point to \mathbf{p} in \mathcal{O}^{3d} . Additionally, we add the hairstyle diffusion prior loss \mathcal{L}_{dif} as in [67] to contain the distribution of the hair geometry texture and address the ambiguity of hair orientations, and the total loss is:

$$\mathcal{L}_{\text{tex}} = \mathcal{L}_{\text{geo}} + \mathcal{L}_{\text{dif}}, \quad (7)$$

After optimizing the geometry texture \mathbf{z} with the above loss, we obtain the coarse hair stand geometries by decoding \mathbf{z} using \mathcal{D} .

4.2. Optimization

To construct the GaussianHair model, we generate N hair strands, each comprising $L = 100$ nodes. This results in a total of N fixed hair roots positioned on the head skin and $N * (L - 1)$ cylinder 3D Gaussians, each containing trainable parameters including the rotation, length, color, and

opacity. We adopt the Stochastic Gradient Descent (SGD) optimizer, following the approach used in 3DGS. To ensure stability in the optimization process and to prevent large-scale oscillatory movements of the hair strands, we employ an exponential decay learning rate scheduler specifically for the rotations and scales. This strategy is crucial in achieving gradual and controlled adjustments to the hair strand geometry, thereby enhancing the realism and accuracy of the final hair model.

We adopt the original photometric loss term in 3DGS as our texture loss:

$$\mathcal{L}_{\text{pho}} = \mathcal{L}_1 + \mathcal{L}_{\text{D-SSIM}}, \quad (8)$$

We enhance our model by accumulating the opacities rendered from GaussianHair into an alpha map, denoted as $\hat{\mathcal{A}}$. To ensure the geometric accuracy of GaussianHair, we enforce consistency between $\hat{\mathcal{A}}$ and the pre-calculated alpha map \mathcal{A} . This supervision through alpha map consistency has been previously demonstrated to be effective in hair/fur modeling contexts, as shown in works like ConvNeRF [41]:

$$\mathcal{L}_{\text{alp}} = \sum_i |\mathcal{A}_i - \hat{\mathcal{A}}_i|, \quad (9)$$

In addition to ensuring alpha map consistency, we also implement a smoothness regularization on the opacities of each single hair strand within the GaussianHair model. This is expressed as:

$$\mathcal{L}_{\text{opa}} = \frac{1}{2} \sum_{i=0}^N \sum_{j=0}^{L-1} (|\alpha_{i,j+1} - \alpha_{i,j}| + |\hat{\alpha}_{i,j+1} - \hat{\alpha}_{i,j}|), \quad (10)$$

where $\alpha_{i,j}$ is the opacity value of j th cylinder Gaussian of the i th strand, and $\hat{\alpha}$ is the difference in opacity of adjacent Gaussians defined by $\alpha_{i,j+1} - \alpha_{i,j}$ along the hair strand. Besides, we apply a strand geometry regularizer to constrain the rotations and scales of adjacent Gaussians to be similar:

$$\mathcal{L}_{\text{pam}} = \sum_{i=0}^N \sum_{j=0}^{L-1} (|\mathbf{d}_{i,j+1} - \mathbf{d}_{i,j}| + |s_{i,j+1} - s_{i,j}|), \quad (11)$$

Thus the total loss function is:

$$\mathcal{L}_{\text{fine}} = \mathcal{L}_{\text{pho}} + \mathcal{L}_{\text{alp}} + \mathcal{L}_{\text{opa}} + \mathcal{L}_{\text{pam}}, \quad (12)$$

During optimization, we observed hair strands mistakenly extending into face and body areas due to hair mask inaccuracies. To resolve this, we initially train head/body Gaussians, isolating the hair region. These head Gaussians are then fixed and rendered with GaussianHair in subsequent steps, allowing for accurate hair modeling without relying on hair masks, and effectively capturing areas missed by incomplete masks.

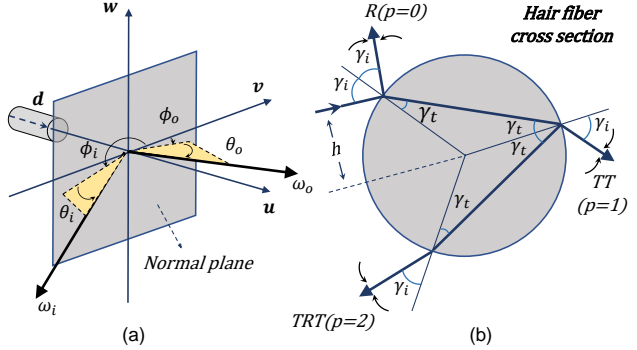


Figure 6. **Illustration of (a) hair fiber scattering geometry and (b) scattering paths.** In (a), it depicts the created coordinate system along with incident direction ω_i and extant direction ω_o . In (b), three types of reflections are considered scattering through a single hair fiber, which are R (specular reflection), TT (transmission through the hair), and TRT (transmission, reflection, and transmission).

To optimize efficiency in modeling and rendering, we implement a strand-wise adaptive density control strategy, reducing the number of redundant cylinder Gaussians that have minimal impact on the final result. This involves pruning strands where a significant proportion of cylindrical Gaussians have negligible opacity, thus avoiding unnecessary computational overhead. Additionally, in regions with high gradient values, we duplicate strands to ensure adequate degrees of freedom, maintaining the integrity and detail of the hair model.

5. GaussianHair Scattering Model

Photorealistic rendering of hair is challenging due to its complex structure and the intricate ways it interacts with light. The visual appearance of hair is significantly influenced by light’s interaction, encompassing both reflection off individual strands and scattering through the hair volume. An effective hair rendering model needs to simulate these complex light interactions, addressing surface reflection, volume scattering, transparency, and shadowing, while also balancing realism with computational efficiency. The Marschner Hair Model, as detailed in Marschner et al.[45], accurately represents light scattering in hair, making it a staple in film and high-end rendering for its realistic outcomes. It categorizes reflections into three types: R (specular reflection), TT (transmission), and TRT (transmission, reflection, transmission). R reflects sharply off hair strands, creating glossy highlights, while TT allows light to pass through a strand, affecting luminosity and color. TRT involves light entering a strand, undergoing internal reflection, and then exiting, yielding softer, deeper highlights. For further details, refer to Fig.6(b) for a visual illustration.

Our reconstructed GaussianHair accurately replicates the

slender structure of hair strands and captures the local diffuse color, particularly under uniform white lighting conditions. The cornerstone of creating a light-aware rendering model lies in incorporating an effective hair scattering model. To this end, we integrate the Marschner Hair Model, which specifically addresses the scattering function of hair fibers. This function is critical in describing how the radiance from a Gaussian primitive is influenced by incident light, thereby enhancing the realism and fidelity of our hair rendering.

5.1. Scattering Parameterization

Hair scattering exhibits anisotropic characteristics, meaning that the way hair fibers reflect light varies significantly along their length as compared to across their width. This anisotropy arises from the elongated, cylindrical shape of hair strands, leading to directional dependence in light reflection and scattering. To quantify this, we use a scattering function $S(\omega_i, \omega_o)$, which describes the distribution of light from an incident direction ω_i to various exitant directions ω_o . The color rendered when viewing from angle ω_o is essentially the cumulative result of light emittance $E(\omega_i)$ attenuated according to this scattering function. This can be mathematically represented as:

$$V(\omega_o) = \sum_{\omega_i} S(\omega_i, \omega_o) E(\omega_i), \quad (13)$$

The Marschner Hair Model [45] articulately formulates the complex hair scattering function $S(\omega_i, \omega_o)$ for an infinitesimally small hair section. It conceptualizes this function as the sum of three components, each of which is further factorized into a longitudinal function $M(\cdot)$ and an azimuthal function $N(\cdot)$. Here, $M(\cdot)$ corresponds to the distribution along the hair’s length, while $N(\cdot)$ pertains to the distribution across its width. To approximate these functions, a coordinate system is established, with the wv plane perpendicular to the hair section and the u axis aligned along it. This allows the longitudinal and azimuthal angles of the incident direction ω_i and the exitant direction ω_o to be defined as (ϕ_i, θ_i) and (ϕ_o, θ_o) , respectively, as illustrated in Fig. 6(a). Consequently, $M(\cdot)$ and $N(\cdot)$ can be represented as functions of these angles:

$$S(\omega_i, \omega_o) = \sum_t M_t(\theta_h) N_t(\theta_d, \phi), \quad t \in \{R, TT, TRT\}, \quad (14)$$

where $\theta_h = (\theta_i + \theta_o)/2$ represents the half longitudinal angle and $\theta_d = (\theta_i - \theta_o)/2$ denotes the half difference angle. The term $t \in \{R, TT, TRT\}$ symbolizes the three components of light scattering paths through a single hair fiber, corresponding to reflection (R), transmission-transmission (TT), and transmission-reflection-transmission (TRT), as depicted in Fig. 6(b).

GaussianHair BSDF Parameterization The rendering process utilizing the Marschner Model necessitates sampling points along hair strands, which involves accurately accumulating various factors including positions along the strands and the angles of light incidence and exitance. This process is inherently computation-intensive. To address this, we adopt the approximated version of the Marschner Model as implemented in the Unreal Engine 4 (UE4). This adaptation significantly enhances rendering speed while maintaining the sophistication of the original model, as discussed in Karis (2016) [24].

In the approximation, the longitudinal scattering components are approximated through sophisticatedly designed functions that depend on the input half longitudinal angle θ_h and adjustable parameters, specifically roughness r and a shift term β . The latter is particularly relevant for the second bound specular shift associated with the TRT component. This relationship is mathematically expressed as:

$$M_t = M_t(\theta_h; r, \beta), \quad t \in \{R, TT, TRT\}, \quad (15)$$

Similarly, for the azimuthal reflection component, the function is determined by the reflection index η , which indicates the proportion of light reflected off the hair surface. This component for the R path is formulated as $N_R = N_R(\theta_d, \phi; \eta)$. The TT and TRT components, on the other hand, are functions of both the base color \mathbf{b} of the hair fiber and the reflection index η . These functions account for the absorption of light as it travels through the hair fiber, and are represented as:

$$N_t = N_t(\theta_d, \phi; \eta, \mathbf{b}), \quad t \in \{TT, TRT\}, \quad (16)$$

This approach enables a more manageable and computationally efficient simulation of hair scattering while still adhering closely to the realistic interaction of light with hair fibers. We use the low-frequency component of the learned spherical harmonics (SH) colors as the base color \mathbf{b} for each cylinder Gaussian in a hair strand. Other physical properties, such as roughness r , shift term β , reflection index η are manually adjustable parameters that control various aspects of the hair’s appearance.

5.2. Multiple Scattering Approximation

The scattering function described earlier pertains to the interaction of light with a single hair strand. However, when considering the entire hair volume, the behavior of light is more complex. Instead of undergoing a single reflection or refraction, light may bounce between multiple strands within the volume before emerging. This multiple scattering effect plays a significant role in capturing the natural appearance of hair. Modeling multi-scattering using ray tracing is computationally intensive. Inspired by the Dual-Scattering method [95], we approximate the multiple

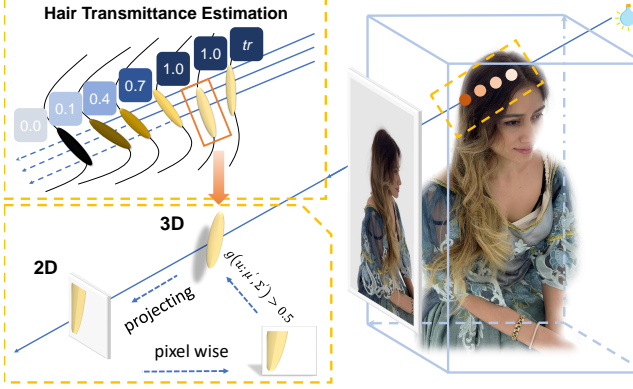


Figure 7. **Hair Transmittance Estimation.** We approximate the light transmittance τ as the inverse of the accumulated opacity T_i of Gaussians from the view of the point light source. Note that for each ray, we select responsible Gaussians with contribution values greater than 0.5.

scattering effect by separating it into two components: the primary scattering component, characterized by light transmittance, and the local scattering component, accounting for multiple internal reflections. Specifically, we calculate how much light passing through a specific hair strand position is attenuated based on the number of hair strands it traverses. Our cylindrical Gaussian representation allows us to estimate light transmittance by considering the accumulated opacity of Gaussians during rasterization.

Primary Scattering We posit that the primary component of multi-scattering originates from the light cast by the source, and for the sake of simpler analysis, we consider a point light source illuminating the hair volume. Once we estimate the light attenuation for each hair strand, we can perform the scattering calculations using Eqn. 13. To achieve this, we introduce an additional transmittance term denoted as τ , which measures how much light has been attenuated to reach a specific Gaussian. We incorporate this term using an additional opacity rendering process.

Specifically, we only consider a point light source for simplicity. We project the 3D hair Gaussians to an image from the viewpoint of the light. We project the 3D hair Gaussians onto an image from the viewpoint of the light source. As illustrated in Fig. 7, we model the decay of transmittance τ from near to far, ranging from 1.0 to 0.0. This decay is calculated as the inverse of transmittance T_i during the rasterization process, and it is assigned to the Gaussians along the ray. Specifically, we determine the responsible Gaussians along the ray based on contribution values that exceed a certain threshold, set at 0.5 in our implementation, i.e., $g(u; \mu', \Sigma') > 0.5$.

Local Scattering Compensation The primary scattering component accounts for the light that reaches the specific Gaussian after undergoing attenuation. However, it is important to note that certain portions of light, which have been scattered by other Gaussians, may also reach the same Gaussian of interest. To address this, we employ a multi-scattering approximation scheme, akin to the approach utilized in the UE4 engine, to address the absence of multiple bounce scattering. More precisely, we interpret the light resulting from multiple bounces as a form of indirect illumination, which reaches the particular Gaussian from all directions, resembling a diffuse effect. This indirect light is subject to attenuation based on the transmittance from the light source (as described in 5.2). Consequently, we model this effect as diffuse color concerning the pseudo-normal of the cylinder Gaussian:

$$\mathbf{n} = \frac{\omega_o - \mathbf{d}(\mathbf{d} \cdot \omega_o)}{\|\omega_o - \mathbf{d}(\mathbf{d} \cdot \omega_o)\|}, \quad (17)$$

where \mathbf{d} is the direction of the cylinder Gaussian. \mathbf{n} is the pseudo normal direction that perpendicular to \mathbf{d} and in the same plane that defined by \mathbf{d} and ω_o . Then the local scattering component is approximated as:

$$S_{local} = \sqrt{\mathbf{b}} \left(\frac{\mathbf{n} \cdot \omega_i + 1}{4\pi} \right) \left(\frac{\mathbf{b}}{L(\mathbf{b})} \right)^\tau, \quad (18)$$

where $L(\mathbf{b})$ is the relative luminance of the base color.

By combining the local scattering component with the primary scattering aforementioned, we derive the final rendering equation for each cylinder Gaussian as:

$$L_o(\omega_o) = \sum_k^K (S(\omega_i^k, \omega_o) + S_{local}(\omega_i^k, \omega_o)) \tau_k L_k, \quad (19)$$

where K is the number of point lights in the virtual environment. L_k is the light intensity of k th light and τ_k is the transmittance obtained from the light pass from k th light. The outgoing radiance L_o is then substituted into Eq. 3 to obtain the final pixel color.

6. Results

In this section, we delineate our datasets and the experimental results. We first report the characteristics of our datasets in terms of quality, diversity, and the approaches employed for processing. We then provide comparisons with prior state-of-the-art methods and evaluation of the main technical components both qualitatively and quantitatively, followed by a detailed showcase of novel applications using our approach. Fig. 8 shows part of our high-fidelity reconstructed hairstyles. The final subsection is devoted to limitations and discussions.



Figure 8. **Gallery of part of our rendering results.** Our method enables the reconstruction of high-fidelity hair rendering results, as demonstrated through a set of diversified hairstyles such as long, short, straight, and curly hair in our showcase. Our high-quality hair reconstruction represents a pivotal component in the advancement of the modeling of high-fidelity digital human assets.



Figure 9. **Data capture.** We use a high-end mobile phone to capture surrounding videos of $4K \times 60$ FPS in a uniformly illuminated environment.

6.1. RealHair Dataset

To facilitate advancements in the field, we have curated an extensive dataset of authentic human hair, comprising 281 high-resolution videos, each spanning approximately 3000 frames. Fig. 9 delineates our sophisticated data capture methodology. Subjects were positioned centrally within our custom-built light dome, facing forward

to ensure consistent, uniform illumination across their hair. High-quality video capture was conducted using advanced mobile phone cameras, capturing intricate hair dynamics and details. Then, our GaussianHair processing technique meticulously preserves the strand geometry and appearance of hair. The uniform lighting setup plays a pivotal role, enabling the captured strands in the dataset to interact with light. These enhancements not only improve the realism of digital hair but also provide seamless integration into existing CG workflows, proving invaluable for downstream applications in computer graphics and animation.

To capture the vast spectrum of hair characteristics such as thickness, curliness, color, and sheen, our dataset embraced a global strategy by engaging models from diverse geographical regions to photograph their natural hair. To enrich the dataset, these models are outfitted in an array of custom-designed costumes during the filming process. These costumes, ranging from traditional to contemporary attire, are carefully selected to complement and accentuate the hairstyles, thus ensuring an authentic representation of various cultural backgrounds. Furthermore, to broaden the scope of our dataset, we enlist professional hairstylists to create a wide variety of unique and culturally significant hairstyles. This collaboration yields an expansive collection of hair types and styles, significantly enhancing the di-

Table 1. Quantitative comparison on appearance.

Method	Case 1			Case 2			Case 3		
	PSNR \uparrow	SSIM \uparrow	LPIPS \downarrow	PSNR \uparrow	SSIM \uparrow	LPIPS \downarrow	PSNR \uparrow	SSIM \uparrow	LPIPS \downarrow
NOPC	24.66	0.8281	0.1917	24.79	0.7264	0.2229	26.61	0.8761	0.1151
MVP	22.38	0.8202	0.2548	23.67	0.7348	0.2773	26.66	0.8777	0.1248
ConvNeRF	27.65	0.8597	0.1553	26.55	0.7246	0.1817	27.93	0.8723	0.0958
3DGS	31.97	0.9226	0.1212	25.93	0.8406	0.1464	29.74	0.9123	0.0643
Ours	29.06	0.9024	0.1371	26.16	0.7550	0.1917	29.54	0.9013	0.0767

versity and applicability of our dataset. To further expand our dataset concerning colored hair, we utilize colored hair wax, allowing for the creation of hairstyles featuring a blend of colors.

Each hair data in our collection also possesses its corresponding tag. To define the hairstyles, we utilized the powerful ChatGPT-4 [52] to extract and analyze the hairstyle features in the images. Specifically, ChatGPT-4 is adopted to label the gender, approximate age range, hairstyle category, hair length range, and hair color for each image. To protect privacy and uphold ethical responsibility, we remove the geographical region information of the subjects, despite we do consider the geographical classification rules in [16]. We welcome the community to contribute additional samples to this dataset. This serves as a valuable contribution to honor traditional culture and broaden the aesthetic standards of the community.

6.2. Comparison

Our comparisons with prior methods are separated into two parts: geometry comparison and appearance comparison. The geometry comparison is conducted qualitatively, adhering to two criteria: whether the geometry texture presents the thin and elongated structure of hair fibers, and whether the geometry texture visually aligns with the reference images. For appearance comparison, we select recent state-of-the-art methods that are at the forefront of hair reconstruction. The comparative analysis encompasses a spectrum of advanced techniques, ensuring a comprehensive and robust evaluation of our approach against prevailing standards.

Comparison on geometry. We compare the reconstructed geometry against the original 3DGS [27] and Neural Haircut [67] on our captured dataset. As illustrated in Fig. 11, we visualize the direction of hair strands. Specifically, for 3DGS and our results, we blend the directions of Gaussian primitives into RGB space. Hair directions in 3DGS are too unorganized and chaotic to present delicate hair structures. Neural Haircut only reconstructs the superficial layer of hair, thereby limiting the intricacy typically associated with hair structures. Our method (Ours-full) adeptly yields visually compelling results of multi-layer and intricate geometric characteristics of hair.

Comparison on appearance. We then compare the reconstructed appearance with NOPC [70], MVP [39], Con-

Table 2. Quantitative ablation on appearance.

Method	PSNR \uparrow	SSIM \uparrow	LPIPS \downarrow
w/o alpha loss (\mathcal{L}_{alp})	25.31	0.8687	0.1570
w/o regularization (\mathcal{L}_{opa})	28.80	0.9013	0.1381
w/o shape optimization	21.72	0.8075	0.1951
full	29.06	0.9024	0.1371

vNeRF [41] and the original 3DGS [27]. As illustrated in Fig. 10, NOPC and MVP fail to achieve high rendering quality and their training is inefficient. ConvNeRF recovers high-frequency details but lacks faithfulness in hair details. 3DGS tends to have blurry artifacts due to their imprecise hair geometry. As for Neural Haircut [67], we fail to replicate comparable results with the open-source code. As shown in Tab. 1, we conduct a quantitative comparison using metrics peak signal-to-noise ratio (PSNR), structural similarity index (SSIM) and Learned Perceptual Image Patch Similarity (LPIPS) with hair masks applied and our method achieves relatively high scores. ConvNeRF sometimes yields better LPIPS scores due to its use of perceptual loss. 3DGS have clear artifacts (e.g. unorganized Gaussian kernels) at the boundary region but can achieve high scores within the hair mask region.

6.3. Evaluation

Here, we further evaluate the technical components of our method to validate their effect on both geometry and appearance. For geometry, we evaluate qualitatively following similar criteria mentioned in the last section. For appearance evaluation, our primary focus centers on the loss terms during the training.

Ablation study on geometry. Qualitative geometric evaluation results are illustrated in Fig. 11 second row. **Ours-ogf** denotes the coarse strand geometry after our initialization process. Compared with our final optimized strand geometry (**Ours-full**), its hair direction is not precise, especially at the termini of hair strands.

Ablation study on appearance. We evaluate our training process with qualitative and quantitative results. As illustrated in Fig. 12, **without alpha loss term** (\mathcal{L}_{alp}), notable artifacts could be observed at the termini of hair strands, which violate the fine, delicate attributes of hair. **Without smoothness regularization term** (\mathcal{L}_{opa}), the optimized hair strands could be observed to have a discontinuity problem, mainly caused by occlusions to various viewpoints during training. If the initialized coarse strand model is fixed **without shape optimization**, then the appearance will be fitted to the coarse geometry, resulting in significant artifacts. As illustrated in Tab. 2, we further adopt PSNR, SSIM, and LPIPS to evaluate the precision with ground truth images. Our full method with all components achieves the best



Figure 10. Qualitative Comparison between NOPC, MVP, ConvNeRF, 3D Gaussian Splatting (3DGS) and our GaussianHair. Our approach reaches a balance between reconstructing delicate hair details and achieving high rendering quality. NOPC and MVP fail to achieve high rendering results, while ConvNeRF and 3DGS have clear artifacts on hair details. Please zoom in on the image for better observation.

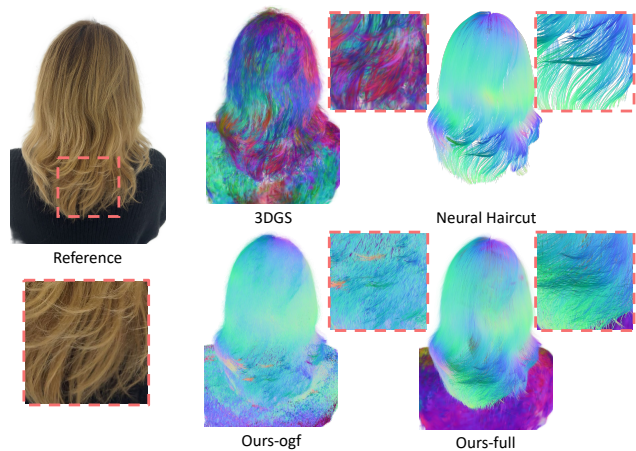


Figure 11. In the first row, we compare the geometry of 3DGS, Neural Haircut, and our method by rendering the strand direction. In the second row, we evaluate the coarse initialized geometry (Ours-ogf) and the final optimized geometry (Ours-full).

score.

6.4. Applications

GaussianHair already facilitates the modeling of plausible hairstyles, coupled with high-fidelity rendering. Yet, our method possesses great potential to be integrated with conventional computer graphics (CG) workflows, supporting applications such as free editing, relighting, and dynamic

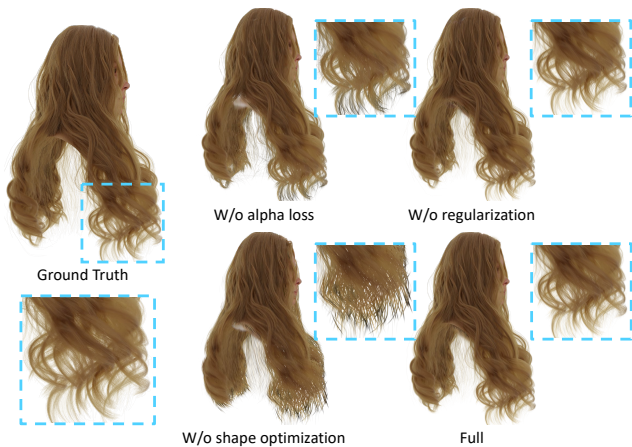


Figure 12. Qualitative evaluation of the training process.

hair rendering. We then depict the applicability in diverse CG contexts.

Editing Once reconstructed, our method naturally facilitates a variety of editing operations, enabling the realization of a virtual salon. Thanks to our strand-based explicit representation, we can naturally adjust the length of strands and hair as illustrated in Fig. 13 column 4. Hair color can also be changed by altering the base color as shown in column 5. Our Gaussian scattering model brings physical attributes

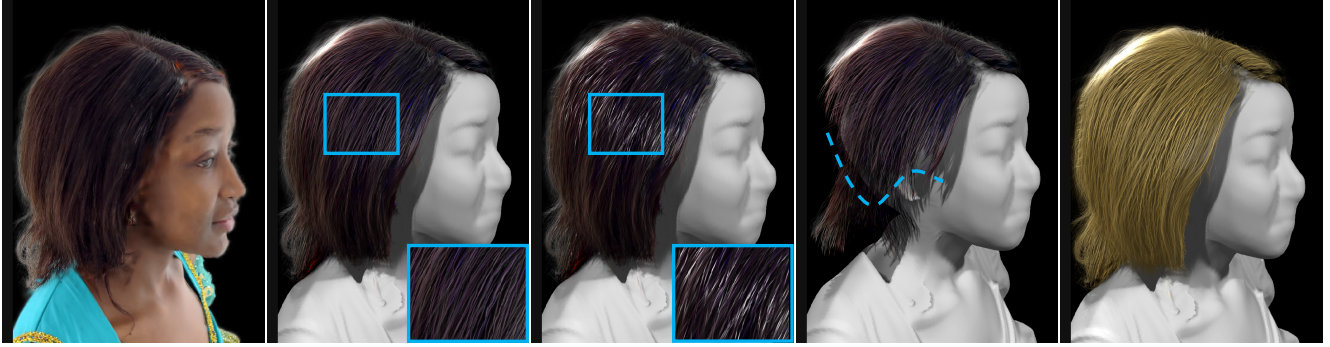


Figure 13. **Editing results.** From left to right: 1. neural rendering results 2. changed lighting 3. roughness adjustment 4. hair cutting 5. base color alteration

to the results and these attributes can be readily modified to simulate various hair textures. As shown in Fig. 13 columns 2&3, hairs appear to be wet after editing roughness under the same lighting condition. These operations can significantly facilitate people in crafting their desired hairstyles.

Relighting The capability to perform high-quality relighting is a critical criterion for whether a method is CG-friendly. As illustrated in Fig. 14, thanks to our Gaussian-Hair scattering model, we can obtain extremely realistic hair rendering results under various light sources. As shown in Fig. 14, we can render with either ordinary composite lighting or film-style illuminations. Note that we combine our reconstructed hair with the face model from ChatAvatar [88, 90]. This enables our method to be seamlessly integrated into the production workflow of the conventional CG pipeline for scene relighting.

Dynamic Hair Rendering Our method is capable of dynamic hair rendering thanks to our strand-based explicit representation. By importing the reconstructed strand model into any conventional CG rendering engine, we can obtain animation results of strands which are then utilized to drive our rendering results. As shown in Fig. 15, the simulated animation of hair being uplifted by wind is utilized to drive our rendering results. With such capability, GaussianHair exhibits the potential to direct integration within an animation production pipeline.

6.5. Discussion and Limitation

Limitation. In this work, GaussianHair has demonstrated its efficacy in modeling hair strands from images, utilizing an innovative approach of initializing and optimizing cylindrical 3D Gaussians. This geometry proxy model adeptly reconstructs the nuanced, thin, and elongated structures of real hair, coupled with a Gaussian scattering model that accurately simulates light interaction. The resultant renderings exhibit impressive lighting details, showcasing the

complex interplay of light and shadow on hair. However, several limitations are identified in our approach. Firstly, the scattering model, as detailed in Sec. 5, deviates from exact physical principles, primarily due to its reliance on an approximated BSDF parameterization from Unreal Engine and a simplified multiple scattering approach. Future improvements could involve integrating a hybrid model that leverages deep learning to enhance the accuracy of the scattering process. Secondly, certain physical properties like roughness and the reflection index are manually adjusted within our model. Optimizing these parameters alongside the hair’s albedo color through neural inverse rendering could potentially yield more accurate results. Thirdly, there is a trade-off between rendering quality and accurate hair geometry representation in our current model. Future research will aim to refine the hair representation for improved results. Lastly, our method faces challenges in modeling complex hairstyles, such as coiled or braided hair, due to the difficulty in reconstructing their internal structures. Future developments could explore the use of generative models to address these complex cases.

Ethics statement. Prior to the collection of our dataset, we established a protocol to ensure informed consent from all participants regarding the usage of the collected data, thereby safeguarding their portrait rights. Our selection of participants adheres to racial and cultural equality and diversity by inviting volunteers from various nationalities and cultural backgrounds. It is significant to note that our dataset is exclusively designated for research purposes, strictly prohibiting any form of commercial usage.

7. Conclusion

In this paper, we introduce GaussianHair, an innovative explicit representation model for human hair, which conceptualizes hair strands as a sequence of interconnected cylindrical 3D Gaussian primitives. GaussianHair excels in cap-

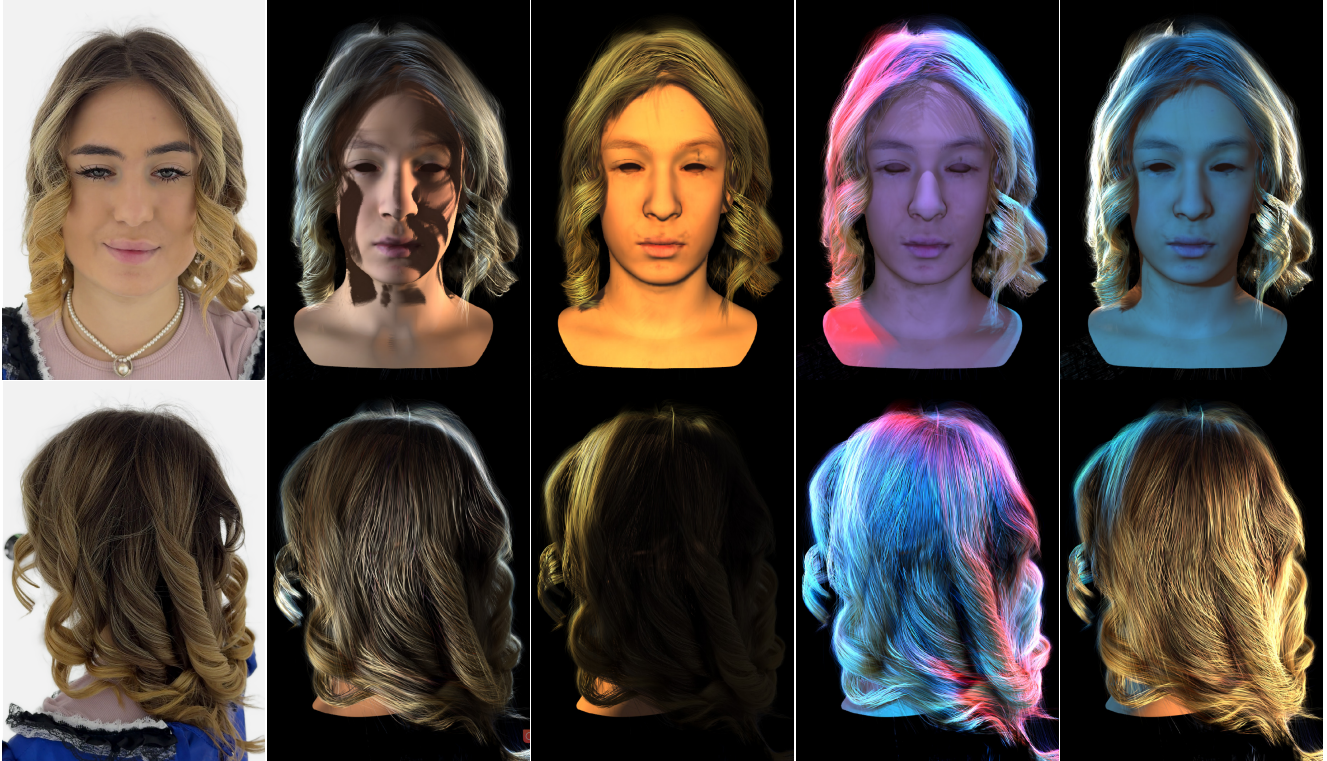


Figure 14. **Relighting.** GaussianHair can render photorealistic relighting results with various lighting conditions. Column 1 is the ground truth reference. Columns 2&3 are rendering results under two ordinary composite lighting. Columns 4&5 show results under Cyber style and "Avatar" style illuminations.



Figure 15. **Dynamic.** After importing our strand model into a conventional CG rendering engine, the returned animation result is then utilized to animate the rendered hair, simulating the effect of wind blowing.

turing intricate hair geometry and appearance, enabling efficient rasterization and high-quality volumetric rendering. Our model integrates the principles of the Marschner Hair Model with advancements from UE4's real-time hair rendering, culminating in the GaussianHair Scattering Model. This model is notable for its realistic rendering, surpassing current limitations in hair reconstruction. Our experiments demonstrate the superior performance of GaussianHair in geometric and appearance fidelity, establishing a new stan-

dard in digital hair reconstruction. Beyond its representation capabilities, GaussianHair is versatile in editing, relighting, and dynamically rendering hair, seamlessly fitting into existing CG pipeline workflows. To complement these technological advancements, we have compiled an extensive dataset of real human hair, representing a wide array of global cultures. This dataset, along with high-resolution videos and GaussianHair geometric representations, aims to promote cultural inclusivity and offer a more accurate rep-

resentation of human diversity.

References

- [1] LLC Agisoft. Agisoft photoscan user manual: professional edition. *St Petersburg, Russia: Agisoft LLC.[Google Scholar]*, 2014. 6
- [2] Ken-ichi Anjyo, Yoshiaki Usami, and Tsuneya Kurihara. A simple method for extracting the natural beauty of hair. In *Proceedings of the 19th annual conference on Computer graphics and interactive techniques*, pages 111–120, 1992. 2
- [3] Yongtang Bao and Yue Qi. Realistic hair modeling from a hybrid orientation field. *The Visual Computer*, 32:729–738, 2016. 4
- [4] Jonathan T Barron, Ben Mildenhall, Matthew Tancik, Peter Hedman, Ricardo Martin-Brualla, and Pratul P Srinivasan. Mip-nerf: A multiscale representation for anti-aliasing neural radiance fields. In *Proceedings of the IEEE/CVF International Conference on Computer Vision*, pages 5855–5864, 2021. 2, 4, 5
- [5] Sai Bi, Zexiang Xu, Pratul Srinivasan, Ben Mildenhall, Kalyan Sunkavalli, Miloš Hašan, Yannick Hold-Geoffroy, David Kriegman, and Ravi Ramamoorthi. Neural reflectance fields for appearance acquisition. *arXiv preprint arXiv:2008.03824*, 2020. 4
- [6] Blender Foundation. Blender, 2023. Version 4.0.2. 2
- [7] Mark Boss, Raphael Braun, Varun Jampani, Jonathan T. Barron, Ce Liu, and Hendrik P.A. Lensch. Nerd: Neural reflectance decomposition from image collections. In *IEEE International Conference on Computer Vision (ICCV)*, 2021. 4
- [8] Ang Cao and Justin Johnson. Hexplane: A fast representation for dynamic scenes. In *Proceedings of the IEEE/CVF Conference on Computer Vision and Pattern Recognition*, pages 130–141, 2023. 4
- [9] Rohan Chabra, Jan E Lenssen, Eddy Ilg, Tanner Schmidt, Julian Straub, Steven Lovegrove, and Richard Newcombe. Deep local shapes: Learning local sdf priors for detailed 3d reconstruction. In *European Conference on Computer Vision*, pages 608–625. Springer, 2020. 4
- [10] Anpei Chen, Zexiang Xu, Andreas Geiger, Jingyi Yu, and Hao Su. Tensorf: Tensorial radiance fields. In *European Conference on Computer Vision*, pages 333–350. Springer, 2022. 4
- [11] Guikun Chen and Wenguan Wang. A survey on 3d gaussian splatting. *arXiv preprint arXiv:2401.03890*, 2024. 4
- [12] Lieu-Hen Chen, Santi Saeyor, Hiroshi Dohi, and Mitsuru Ishizuka. A system of 3d hair style synthesis based on the wisp model. *The Visual Computer*, 15:159–170, 1999. 3
- [13] Byoungwon Choe and Hyeong-Seok Ko. A statistical wisp model and pseudophysical approaches for interactive hairstyle generation. *IEEE Transactions on Visualization and Computer Graphics*, 11(2):160–170, 2005. 3
- [14] Steven J Gortler, Radek Grzeszczuk, Richard Szeliski, and Michael F Cohen. The lumigraph. In *Seminal Graphics Papers: Pushing the Boundaries, Volume 2*, pages 453–464. 2023. 5
- [15] Stéphane Grabli, François X Sillion, Stephen R Marschner, and Jerome E Lengyel. Image-based hair capture by inverse lighting. In *Proceedings of Graphics Interface (GI)*, pages 51–58, 2002. 4
- [16] Harvard. Racial/ethnic classifications. https://hr.harvard.edu/files/humanresources/files/race_ethnicity_definitions_2014.pdf, 2014. 12
- [17] Tong He, Yuanlu Xu, Shunsuke Saito, Stefano Soatto, and Tony Tung. Arch++: Animation-ready clothed human reconstruction revisited. In *Proceedings of the IEEE/CVF International Conference on Computer Vision*, pages 11046–11056, 2021. 4
- [18] Jerry Hsu, Tongtong Wang, Zherong Pan, Xifeng Gao, Cem Yuksel, and Kui Wu. Sag-free initialization for strand-based hybrid hair simulation. *ACM Transactions on Graphics (Proceedings of SIGGRAPH 2023)*, 42(4), 2023. 2
- [19] Liwen Hu, Chongyang Ma, Linjie Luo, and Hao Li. Robust hair capture using simulated examples. *ACM Transactions on Graphics (TOG)*, 33(4):1–10, 2014. 4
- [20] Liwen Hu, Chongyang Ma, Linjie Luo, and Hao Li. Single-view hair modeling using a hairstyle database. *ACM Transactions on Graphics (ToG)*, 34(4):1–9, 2015. 4
- [21] Liwen Hu, Derek Bradley, Hao Li, and Thabo Beeler. Simulation-ready hair capture. In *Computer Graphics Forum*, pages 281–294. Wiley Online Library, 2017. 2
- [22] Zeng Huang, Yuanlu Xu, Christoph Lassner, Hao Li, and Tony Tung. Arch: Animatable reconstruction of clothed humans. In *Proceedings of the IEEE/CVF Conference on Computer Vision and Pattern Recognition*, pages 3093–3102, 2020. 4
- [23] Chiyu Jiang, Avneesh Sud, Ameesh Makadia, Jingwei Huang, Matthias Nießner, Thomas Funkhouser, et al. Local implicit grid representations for 3d scenes. In *Proceedings of the IEEE/CVF Conference on Computer Vision and Pattern Recognition*, pages 6001–6010, 2020. 4
- [24] Brian Karis. Physically based hair shading in unreal. In *SIGGRAPH '16*, 2016. 9
- [25] Tero Karras, Timo Aila, Samuli Laine, and Jaakko Lehtinen. Progressive growing of gans for improved quality, stability, and variation. In *International Conference on Learning Representations*, 2018. 4
- [26] Tero Karras, Samuli Laine, and Timo Aila. A style-based generator architecture for generative adversarial networks. In *Proceedings of the IEEE/CVF conference on computer vision and pattern recognition*, pages 4401–4410, 2019. 4
- [27] Bernhard Kerbl, Georgios Kopanas, Thomas Leimkühler, and George Drettakis. 3d gaussian splatting for real-time radiance field rendering. *ACM Transactions on Graphics*, 42(4), 2023. 2, 4, 5, 6, 12
- [28] Tae-Yong Kim and Ulrich Neumann. Interactive multiresolution hair modeling and editing. *ACM Transactions on Graphics (TOG)*, 21(3):620–629, 2002. 3
- [29] Alexander Kirillov, Eric Mintun, Nikhila Ravi, Hanzi Mao, Chloe Rolland, Laura Gustafson, Tete Xiao, Spencer Whitehead, Alexander C. Berg, Wan-Yen Lo, Piotr Dollár, and Ross Girshick. Segment anything. *arXiv:2304.02643*, 2023. 6

- [30] Chuan Koon Koh and Zhiyong Huang. Real-time animation of human hair modeled in strips. In *Computer Animation and Simulation 2000: Proceedings of the Eurographics Workshop in Interlaken, Switzerland, August 21–22, 2000*, pages 101–110. Springer, 2000. 3
- [31] Waiming Kong and Masayuki Nakajima. Generation of 3d hair model from multiple pictures. *The Journal of the Institute of Image Information and Television Engineers*, 52(9): 1351–1356, 1998. 4
- [32] Zhiyi Kuang, Yiyang Chen, Hongbo Fu, Kun Zhou, and Youyi Zheng. Deepmvshair: Deep hair modeling from sparse views. In *SIGGRAPH Asia 2022 Conference Papers*, pages 1–8, 2022. 4
- [33] Chloe LeGendre, Loc Hyunh, Shanhe Wang, and Paul Debevec. Modeling vellus facial hair from asperity scattering silhouettes. In *ACM SIGGRAPH 2017 Talks*, pages 1–2. 2017. 2
- [34] Marc Levoy and Pat Hanrahan. Light field rendering. In *Seminal Graphics Papers: Pushing the Boundaries, Volume 2*, pages 441–452. 2023. 5
- [35] Tianye Li, Timo Bolkart, Michael J. Black, Hao Li, and Javier Romero. Learning a model of facial shape and expression from 4D scans. *ACM Transactions on Graphics (Proc. SIGGRAPH Asia)*, 36(6):194:1–194:17, 2017. 6
- [36] Wenqi Liang and Zhiyong Huang. An enhanced framework for real-time hair animation. In *11th Pacific Conference on Computer Graphics and Applications, 2003. Proceedings.*, pages 467–471. IEEE, 2003. 3
- [37] Lingjie Liu, Jiatao Gu, Kyaw Zaw Lin, Tat-Seng Chua, and Christian Theobalt. Neural sparse voxel fields. *Advances in Neural Information Processing Systems*, 33:15651–15663, 2020. 4
- [38] Shilong Liu, Zhaoyang Zeng, Tianhe Ren, Feng Li, Hao Zhang, Jie Yang, Chunyuan Li, Jianwei Yang, Hang Su, Jun Zhu, et al. Grounding dino: Marrying dino with grounded pre-training for open-set object detection. *arXiv preprint arXiv:2303.05499*, 2023. 6
- [39] Stephen Lombardi, Tomas Simon, Gabriel Schwartz, Michael Zollhoefer, Yaser Sheikh, and Jason Saragih. Mixture of volumetric primitives for efficient neural rendering. *ACM Trans. Graph.*, 40(4), 2021. 12
- [40] Stephen Lombardi, Tomas Simon, Gabriel Schwartz, Michael Zollhoefer, Yaser Sheikh, and Jason Saragih. Mixture of volumetric primitives for efficient neural rendering. *ACM Transactions on Graphics (TOG)*, 40(4):1–13, 2021. 4
- [41] H. Luo, A. Chen, Q. Zhang, B. Pang, M. Wu, L. Xu, and J. Yu. Convolutional neural opacity radiance fields. In *2021 IEEE International Conference on Computational Photography (ICCP)*, pages 1–12, Los Alamitos, CA, USA, 2021. IEEE Computer Society. 4, 8, 12
- [42] Haimin Luo, Teng Xu, Yuheng Jiang, Chenglin Zhou, Qiwei Qiu, Yingliang Zhang, Wei Yang, Lan Xu, and Jingyi Yu. Artemis: Articulated neural pets with appearance and motion synthesis. *ACM Trans. Graph.*, 41(4), 2022. 4
- [43] Linjie Luo, Hao Li, Sylvain Paris, Thibaut Weise, Mark Pauly, and Szymon Rusinkiewicz. Multi-view hair capture using orientation fields. In *2012 IEEE Conference on Computer Vision and Pattern Recognition*, pages 1490–1497. IEEE, 2012. 4, 5
- [44] Linjie Luo, Cha Zhang, Zhengyou Zhang, and Szymon Rusinkiewicz. Wide-baseline hair capture using strand-based refinement. In *Proceedings of the IEEE Conference on Computer Vision and Pattern Recognition*, pages 265–272, 2013. 4, 5
- [45] Stephen R. Marschner, Henrik Wann Jensen, Mike Cammarano, Steve Worley, and Pat Hanrahan. Light scattering from human hair fibers. *ACM Trans. Graph.*, 22(3):780–791, 2003. 3, 8, 9
- [46] Ricardo Martin-Brualla, Noha Radwan, Mehdi SM Sajjadi, Jonathan T Barron, Alexey Dosovitskiy, and Daniel Duckworth. Nerf in the wild: Neural radiance fields for unconstrained photo collections. In *Proceedings of the IEEE/CVF Conference on Computer Vision and Pattern Recognition*, pages 7210–7219, 2021. 4
- [47] Lars Mescheder, Michael Oechsle, Michael Niemeyer, Sebastian Nowozin, and Andreas Geiger. Occupancy networks: Learning 3d reconstruction in function space. In *Proceedings of the IEEE/CVF Conference on Computer Vision and Pattern Recognition*, pages 4460–4470, 2019. 4
- [48] Ben Mildenhall, Pratul P Srinivasan, Matthew Tancik, Jonathan T Barron, Ravi Ramamoorthi, and Ren Ng. Nerf: Representing scenes as neural radiance fields for view synthesis. *Communications of the ACM*, 65(1):99–106, 2021. 2, 4, 5
- [49] Thomas Müller, Alex Evans, Christoph Schied, and Alexander Keller. Instant neural graphics primitives with a multiresolution hash encoding. *ACM Trans. Graph.*, 41(4):102:1–102:15, 2022. 2, 4, 5
- [50] Giljoo Nam, Chenglei Wu, Min H Kim, and Yaser Sheikh. Strand-accurate multi-view hair capture. In *Proceedings of the IEEE/CVF Conference on Computer Vision and Pattern Recognition*, pages 155–164, 2019. 2, 4
- [51] Paul Noble and Wen Tang. Modelling and animating cartoon hair with nurbs surfaces. In *Proceedings Computer Graphics International, 2004.*, pages 60–67. IEEE, 2004. 3
- [52] OpenAI. Chatgpt: A large-scale generative language model. 2022. 12
- [53] Sylvain Paris, Hector M. Briceño, and François X. Sillion. Capture of hair geometry from multiple images. In *ACM SIGGRAPH 2004 Papers*, page 712–719, New York, NY, USA, 2004. Association for Computing Machinery. 6
- [54] Sylvain Paris, Hector M Briceno, and François X Sillion. Capture of hair geometry from multiple images. *ACM transactions on graphics (TOG)*, 23(3):712–719, 2004. 4
- [55] Sylvain Paris, Will Chang, Oleg I Kozhushnyan, Wojciech Jarosz, Wojciech Matusik, Matthias Zwicker, and Frédo Durand. Hair photobooth: geometric and photometric acquisition of real hairstyles. *ACM Trans. Graph.*, 27(3):30, 2008. 4, 5
- [56] Jeong Joon Park, Peter Florence, Julian Straub, Richard Newcombe, and Steven Lovegrove. DeepSDF: Learning continuous signed distance functions for shape representation. In *Proceedings of the IEEE/CVF Conference on Computer Vision and Pattern Recognition*, pages 165–174, 2019. 4

- [57] Keunhong Park, Utkarsh Sinha, Peter Hedman, Jonathan T. Barron, Sofien Bouaziz, Dan B Goldman, Ricardo Martin-Brualla, and Steven M. Seitz. Hypernerf: A higher-dimensional representation for topologically varying neural radiance fields. *ACM Trans. Graph.*, 40(6), 2021. 4
- [58] Deborah Patrick, Shaun Bangay, and Adele Lobb. Modelling and rendering techniques for african hairstyles. In *Proceedings of the 3rd international conference on Computer graphics, virtual reality, visualisation and interaction in Africa*, pages 115–124, 2004. 3
- [59] Songyou Peng, Michael Niemeyer, Lars Mescheder, Marc Pollefeys, and Andreas Geiger. Convolutional occupancy networks. In *Computer Vision—ECCV 2020: 16th European Conference, Glasgow, UK, August 23–28, 2020, Proceedings, Part III 16*, pages 523–540. Springer, 2020. 4
- [60] Sida Peng, Yuanqing Zhang, Yinghao Xu, Qianqian Wang, Qing Shuai, Hujun Bao, and Xiaowei Zhou. Neural body: Implicit neural representations with structured latent codes for novel view synthesis of dynamic humans. In *Proceedings of the IEEE/CVF Conference on Computer Vision and Pattern Recognition*, pages 9054–9063, 2021. 4
- [61] Robert E Rosenblum, Wayne E Carlson, and Edwin Tripp III. Simulating the structure and dynamics of human hair: modelling, rendering and animation. *The Journal of Visualization and Computer Animation*, 2(4):141–148, 1991. 2
- [62] Radu Alexandru Rosu, Shunsuke Saito, Ziyang Wang, Chenglei Wu, Sven Behnke, and Giljoo Nam. Neural strands: Learning hair geometry and appearance from multi-view images. In *European Conference on Computer Vision*, pages 73–89. Springer, 2022. 2, 4, 5, 7
- [63] Shunsuke Saito, Liwen Hu, Chongyang Ma, Hikaru Ibayashi, Linjie Luo, and Hao Li. 3d hair synthesis using volumetric variational autoencoders. *ACM Transactions on Graphics (TOG)*, 37(6):1–12, 2018. 4
- [64] Shunsuke Saito, Zeng Huang, Ryota Natsume, Shigeo Morishima, Angjoo Kanazawa, and Hao Li. Pifu: Pixel-aligned implicit function for high-resolution clothed human digitization. In *Proceedings of the IEEE/CVF International Conference on Computer Vision*, pages 2304–2314, 2019. 4
- [65] Johannes L Schonberger and Jan-Michael Frahm. Structure-from-motion revisited. In *Proceedings of the IEEE conference on computer vision and pattern recognition*, pages 4104–4113, 2016. 6
- [66] Yuefan Shen, Shunsuke Saito, Ziyang Wang, Olivier Maury, Chenglei Wu, Jessica Hodgins, Youyi Zheng, and Giljoo Nam. Ct2hair: High-fidelity 3d hair modeling using computed tomography. *ACM Transactions on Graphics*, 42(4):1–13, 2023. 4
- [67] Vanessa Sklyarova, Jenya Chelischev, Andreea Dogaru, Igor Medvedev, Victor Lempitsky, and Egor Zakharov. Neural haircut: Prior-guided strand-based hair reconstruction. *arXiv preprint arXiv:2306.05872*, 2023. 2, 3, 4, 5, 6, 7, 12
- [68] Tiancheng Sun, Giljoo Nam, Carlos Aliaga, Christophe Hery, and Ravi Ramamoorthi. Human hair inverse rendering using multi-view photometric data. 2021. 2, 4
- [69] Dor Verbin, Peter Hedman, Ben Mildenhall, Todd Zickler, Jonathan T. Barron, and Pratul P. Srinivasan. Ref-NeRF: Structured view-dependent appearance for neural radiance fields. *CVPR*, 2022. 4
- [70] Cen Wang, Minye Wu, Ziyu Wang, Liao Wang, Hao Sheng, and Jingyi Yu. Neural opacity point cloud. *IEEE Transactions on Pattern Analysis and Machine Intelligence*, 42(7):1570–1581, 2020. 2, 5, 12
- [71] Peng Wang, Lingjie Liu, Yuan Liu, Christian Theobalt, Taku Komura, and Wenping Wang. Neus: Learning neural implicit surfaces by volume rendering for multi-view reconstruction. In *35th Conference on Neural Information Processing Systems*, pages 27171–27183. Curran Associates, Inc., 2021. 4
- [72] Tao Wang and Xue Dong Yang. Hair design based on the hierarchical cluster hair model. *Geometric modeling: techniques, applications, systems and tools*, pages 329–359, 2004. 3
- [73] Yiming Wang, Qin Han, Marc Habermann, Kostas Daniilidis, Christian Theobalt, and Lingjie Liu. Neus2: Fast learning of neural implicit surfaces for multi-view reconstruction. In *Proceedings of the IEEE/CVF International Conference on Computer Vision*, pages 3295–3306, 2023. 4
- [74] Ziyang Wang, Giljoo Nam, Tsur Stuyck, Stephen Lombardi, Michael Zollhöfer, Jessica Hodgins, and Christoph Lassner. Hvh: Learning a hybrid neural volumetric representation for dynamic hair performance capture. In *Proceedings of the IEEE/CVF Conference on Computer Vision and Pattern Recognition*, pages 6143–6154, 2022. 4, 5
- [75] Ziyang Wang, Giljoo Nam, Tsur Stuyck, Stephen Lombardi, Chen Cao, Jason Saragih, Michael Zollhöfer, Jessica Hodgins, and Christoph Lassner. Neuwigs: A neural dynamic model for volumetric hair capture and animation. In *Proceedings of the IEEE/CVF Conference on Computer Vision and Pattern Recognition*, pages 8641–8651, 2023. 4, 5
- [76] Zian Wang, Tianchang Shen, Merlin Nimier-David, Nicholas Sharp, Jun Gao, Alexander Keller, Sanja Fidler, Thomas Müller, and Zan Gojcic. Adaptive shells for efficient neural radiance field rendering. *ACM Trans. Graph.*, 42(6), 2023. 5
- [77] Yichen Wei, Eyal Ofek, Long Quan, and Heung-Yeung Shum. Modeling hair from multiple views. In *ACM SIGGRAPH 2005 Papers*, pages 816–820. 2005. 4, 5
- [78] Keyu Wu, Yifan Ye, Lingchen Yang, Hongbo Fu, Kun Zhou, and Youyi Zheng. Neuralhdhair: Automatic high-fidelity hair modeling from a single image using implicit neural representations. In *Proceedings of the IEEE/CVF Conference on Computer Vision and Pattern Recognition*, pages 1526–1535, 2022. 4
- [79] Zhan Xu and Xue Dong Yang. V-hairstudio: an interactive tool for hair design. *IEEE Computer Graphics and Applications*, 21(3):36–43, 2001. 3
- [80] Lingchen Yang, Zefeng Shi, Youyi Zheng, and Kun Zhou. Dynamic hair modeling from monocular videos using deep neural networks. *ACM Transactions on Graphics (TOG)*, 38(6):1–12, 2019. 4
- [81] Xue Dong Yang, Zhan Xu, Jun Yang, and Tao Wang. The cluster hair model. *Graphical Models*, 62(2):85–103, 2000. 3
- [82] Yao Yao, Jingyang Zhang, Jingbo Liu, Yihang Qu, Tian Fang, David McKinnon, Yanghai Tsin, and Long Quan.

- Neif: Neural incident light field for physically-based material estimation. In *European Conference on Computer Vision*, pages 700–716. Springer, 2022. 4
- [83] Alex Yu, Ruilong Li, Matthew Tancik, Hao Li, Ren Ng, and Angjoo Kanazawa. Plenotrees for real-time rendering of neural radiance fields. In *Proceedings of the IEEE/CVF International Conference on Computer Vision*, pages 5752–5761, 2021. 4
- [84] Xuan Yu, Zhan Yu, Xiaogang Chen, and Jingyi Yu. A hybrid image-cad based system for modeling realistic hairstyles. In *Proceedings of the 18th meeting of the ACM SIGGRAPH Symposium on Interactive 3D Graphics and Games*, pages 63–70, 2014. 4
- [85] Cem Yuksel and Sarah Tariq. Advanced techniques in real-time hair rendering and simulation. In *ACM SIGGRAPH 2010 Courses*, pages 1:1–1:168, New York, NY, USA, 2010. ACM. 2
- [86] Cem Yuksel, Scott Schaefer, and John Keyser. Hair meshes. *ACM Transactions on Graphics (TOG)*, 28(5):1–7, 2009. 3
- [87] Jingyang Zhang, Yao Yao, Shiwei Li, Jingbo Liu, Tian Fang, David McKinnon, Yanghai Tsin, and Long Quan. Neif++: Inter-reflectable light fields for geometry and material estimation. *arXiv preprint arXiv:2303.17147*, 2023. 4
- [88] Longwen Zhang, Qiwei Qiu, Hongyang Lin, Qixuan Zhang, Cheng Shi, Wei Yang, Ye Shi, Sibe Yang, Lan Xu, and Jingyi Yu. Dreamface: Progressive generation of animatable 3d faces under text guidance. *ACM Trans. Graph.*, 42(4), 2023. 14
- [89] Meng Zhang, Menglei Chai, Hongzhi Wu, Hao Yang, and Kun Zhou. A data-driven approach to four-view image-based hair modeling. *ACM Trans. Graph.*, 36(4):156–1, 2017. 4
- [90] Qixuan Zhang, Longwen Zhang, Lan Xu, Di Wu, and Jingyi Yu. Chatavatar: Creating hyper-realistic physically-based 3d facial assets through ai-driven conversations. In *ACM SIGGRAPH 2023 Real-Time Live!, SIGGRAPH 2023, Los Angeles, CA, USA, August 6-10, 2023*, pages 1:1–1:2. ACM, 2023. 14
- [91] Xiuming Zhang, Pratul P Srinivasan, Boyang Deng, Paul Debevec, William T Freeman, and Jonathan T Barron. Nerfactor: Neural factorization of shape and reflectance under an unknown illumination. *ACM Transactions on Graphics (TOG)*, 40(6):1–18, 2021. 4
- [92] Fuqiang Zhao, Yuheng Jiang, Kaixin Yao, Jiakai Zhang, Liao Wang, Haizhao Dai, Yuhui Zhong, Yingliang Zhang, Minye Wu, Lan Xu, et al. Human performance modeling and rendering via neural animated mesh. *ACM Transactions on Graphics (TOG)*, 41(6):1–17, 2022. 4, 6
- [93] Yujian Zheng, Zirong Jin, Moran Li, Haibin Huang, Chongyang Ma, Shuguang Cui, and Xiaoguang Han. Hairstep: Transfer synthetic to real using strand and depth maps for single-view 3d hair modeling. In *Proceedings of the IEEE/CVF Conference on Computer Vision and Pattern Recognition*, pages 12726–12735, 2023. 4
- [94] Yi Zhou, Liwen Hu, Jun Xing, Weikai Chen, Han-Wei Kung, Xin Tong, and Hao Li. Hairnet: Single-view hair reconstruction using convolutional neural networks. In *Proceedings of the European Conference on Computer Vision (ECCV)*, pages 235–251, 2018. 4
- [95] Arno Zinke, Cem Yuksel, Andreas Weber, and John Keyser. Dual scattering approximation for fast multiple scattering in hair. *ACM Trans. Graph.*, 27(3):1–10, 2008. 9